NUCL SCI TECH (2018) 29:54
https://doi.org/10.1007/s41365-018-0393-1

Ω and ϕ production in Au + Au collisions at $\sqrt{s_{NN}} = 11.5$ and 7.7 GeV in a dynamical quark coalescence model

Xiao-Hai Jin[1,2] · Jin-Hui Chen[1] · Yu-Gang Ma[1,3] · Song Zhang[1] · Chun-Jian Zhang[1,2] · Chen Zhong[1]

Received: 3 January 2018 / Revised: 28 January 2018 / Accepted: 18 February 2018 / Published online: 16 March 2018

Abstract The Ω and ϕ production in relativistic heavy-ion collisions is studied in a dynamical quark coalescence model using the phase space information of strange quarks from a multiphase transport (AMPT) model. Enhanced local parton density fluctuation is implemented in the AMPT to simulate the QCD phase transition dynamics. By studying the transverse momentum p_T spectra and the elliptic flow of the multi-strangeness particles, such as Ω and ϕ, and the Ω/ϕ ratio as a function of p_T in the AMPT, we find that the new development improves the description of experimental data. The study motivates further experimental investigations of Ω and ϕ production in phase II of the Beam Energy Scan program at RHIC.

Keywords QCD phase transition · Multi-strangeness particles · Elliptic flow · AMPT

This work was supported in part by the Major State Basic Research Development Program in China (Nos. 2014CB845400 and 2015CB856904), and the National Natural Science Foundation of China (Nos. 11775288, 11421505, and 11520101004).

✉ Jin-Hui Chen
chenjinhui@sinap.ac.cn

Yu-Gang Ma
ygma@sinap.ac.cn

1 Shanghai Institute of Applied Physics, Chinese Academy of Sciences, Shanghai 201800, China

2 University of Chinese Academy of Sciences, Beijing 100049, China

3 ShanghaiTech University, Shanghai 200031, China

1 Introduction

Searching for the QCD critical point and mapping the QCD phase diagram are major scientific goals of the Beam Energy Scan (BES) program at Relativistic Heavy-Ion Collider (RHIC) [1]. Finite temperature lattice QCD calculations show that at high temperature and low baryon chemical potential (μ_B), a phase transition from hadron gas to the quark gluon plasma (QGP) will happen, and the phase transition is smooth and continuous [2]. At large μ_B region, the QCD-based models predict that the phase transition is of the first order and there should exist a QCD critical point as the endpoint of the first order phase boundary [3–5].

Heavy-ion collisions at relativistic energy provide a unique opportunity to study the properties of QGP and the QCD phase diagram. Many exciting results in the field show rich structure of QCD matter, such as the non-monotonic behavior of conserved quantity fluctuation and final state correlations [6–15], net-proton direct flow [16], the strangeness enhancement [17–20], the local baryon-strangeness correlation measurement from the hypernuclei system [21–23], novel quantum phenomena induced by strong magnetic fields in heavy-ion collisions [24], the breaking of the number of constituent quark scaling on identified particles [25–27], and the deviation of the Ω/ϕ ratio in BES in comparison with data at top RHIC energy [28].

Multi-strange hadrons, such as Ω and ϕ, are clean probes to explore the QCD phase diagram [29, 30], as they are expected to have a relatively small hadronic interaction cross section and little contribution from resonance decay [31, 32]. Therefore, they can carry the information directly from the chemical freeze-out stage with little or no distortion due to hadronic rescattering. As a result, the production of Ω and ϕ particles offers an advantage in probing the transition from partonic to hadronic dynamics [29]. In a recent measurement of Ω and ϕ production at midrapidity from Au + Au collisions at $\sqrt{s_{\mathrm{NN}}}$ = 7.7, 11.5, 19.6, 27, and 39 GeV from the STAR experiment at RHIC, one finds that the Ω/ϕ ratios scaled by their number of constituent quark show a suppression of strange quark production in central collisions at 11.5 GeV compared to results at $\sqrt{s_{\mathrm{NN}}} \geq$ 19.6 GeV, and the data of 19.6 GeV or above show little beam energy dependence, which may suggest strange quark equilibration is achieved in higher energy but not in lower energy [28]. We have carried out a detail study on the underlying dynamics of strange quark matter at the RHIC based on AMPT model previously and found that the AMPT model presents the trend of Ω/ϕ versus p_{T} of the data, though under-predicts the Ω yield by a factor of 5 [30]. New development of the naive quark coalescence model in the AMPT model improves the description of baryon production in heavy-ion collisions, such as protons and Λ, but still significantly under-predicts the Ω and Ξ yield [33]. An alternative solution using a dynamical quark coalescence model to replace the naive quark coalescence model in the AMPT model predicted the Ω and ϕ yield in Au + Au collisions at $\sqrt{s_{\mathrm{NN}}}$ = 200 GeV reasonably well [34]. In this paper, we follow the procedure described in Ref. [34] and introduce the local parton density fluctuation effect in the AMPT model to study the Ω and ϕ production as a possible signal of the QCD phase transition. We noted that similar idea was discussed in Ref. [35].

2 The AMPT model

The AMPT model is a hybrid model developed to describe heavy-ion collisions at relativistic energies [36]. It has two versions: default AMPT and string melting AMPT. In our study, we adopt the string melting version to study the QCD fluctuation effect. In the string melting version, all excited strings are converted into partons [36], it has a clear advantage over the default version in describing the flow of harmonic and pion interferometry [33, 37–39]. The AMPT model with the string melting scenario consists of four components. The initial stage is described by a heavy-ion jet interaction generator (HIJING) [40, 41], which is designed to simulate multiple jets and particle production in heavy-ion collisions. Zhang's parton cascade (ZPC) [42] is used to describe scattering among partons. It only included two-body elastic interaction until now. The hadronization of parton is based on a naive quark coalescence model from coordinate space distribution [36]. The scattering of resulting hadrons is described by a relativistic transport (ART) model [43, 44].

In the transport approach, interactions among partons are described by their scattering cross sections, which in the AMPT model are given by [42]

$$\frac{\mathrm{d}\sigma_{\mathrm{p}}}{\mathrm{d}t} \simeq \frac{9\pi\alpha_{\mathrm{s}}^2}{2(t-\mu^2)^2}, \tag{1}$$

$$\sigma_{\mathrm{p}} \simeq \frac{9\pi\alpha_{\mathrm{s}}^2}{2\mu^2}\frac{1}{1+\mu^2/s}. \tag{2}$$

where α_{s} is the strong coupling constant with a typical value of 0.47 in AMPT, μ is the screening mass which depends on the medium effect [42], and s and t are the usual Mandelstam variables. By applying a large parton scattering cross sections of 6–10 mb, the AMPT model can reproduce the centrality and transverse momentum dependence of hadron elliptic flow [45]. Recent development on the input parameters of AMPT model seems to obtain a smaller value, and more close to the value used in pQCD calculation [38]. For our current study, we follow the instruction from Ref. [38] and take the parton scattering cross section of 3 mb to simulate parton interaction.

In order to understand the QCD phase diagram on a wide range of collision energies, we add local parton density fluctuation in AMPT. Viewed from the thermodynamics, a critical point is a point at which a single thermodynamic state bifurcates into two macroscopically distinct states. This bifurcation may lead to long-range thermal fluctuations. To model this effect, a large density fluctuation is introduced in the end of parton scattering in ZPC. Specifically, we assume that the partonic matter prior to the QCD phase transition consists of clusters of various sizes. We redistribute partons produced in the AMPT model to a few clusters but keep their momenta unchanged. In our algorithm, the center of a cluster is determined by the maximum number density of parton distributions in that event. Cluster positions are selected based on the freeze-out positions of partons, and then far away partons in the transverse plane are moved close to the nearest cluster. All partons then coalescence into hadrons. To demonstrate this effect, we only allow in the present study the formation of four quark clusters before hadronization. An example of the parton spatial distribution is shown in panel (b) of Fig. 1. For comparison, the distribution from the AMPT model is shown in panel (a). The subsequent distribution of hadrons formed immediately after hadronization from partons is shown in panel (c) and (d), respectively. From Fig. 1, it is seen that the enhanced local parton density fluctuation has a clear effect on the spatial distributions of hadronic matter in AMPT. The fluctuation effect (panel d) is stronger than the original AMPT model (panel c). In this

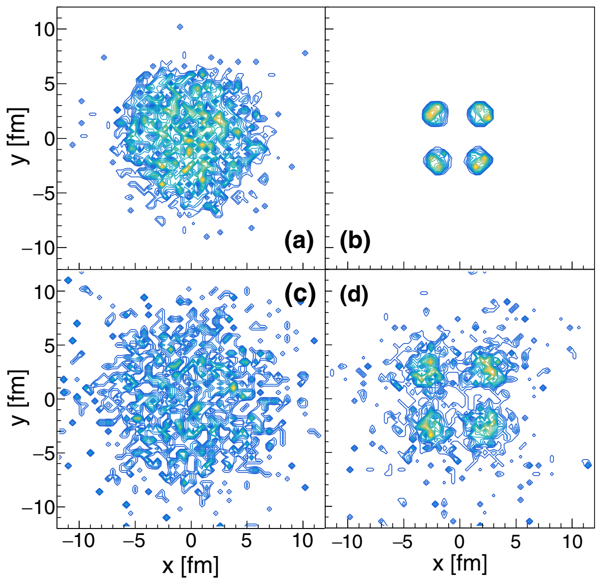

Fig. 1 (Color online) Spatial distributions of partons and hadrons in the transverse plane from an AMPT event in Au + Au collisions at $\sqrt{s_{\mathrm{NN}}}$ = 11.5 GeV. **a**, **b** Distributions of partons from AMPT with a string melting scenario and AMPT with enhanced local parton density fluctuation scenario, respectively. **c**, **d** Distributions of hadrons accordingly

paper, we do our calculations with string melting AMPT in version 2.24 for Au + Au collision.

3 The dynamical quark coalescence model of Ω and ϕ

A dynamical quark coalescence model has been used to study the production of Ω and ϕ [34]. In this model, the probability for producing a hadron from partons is given by the overlap of parton phase space distributions with the parton Wigner function inside the hadron [46]. The multiplicity of a M-parton hadron in an heavy-ion collision is given by

$$N_M = G \int \mathrm{d}\mathbf{r}_{i_1} \mathrm{d}\mathbf{q}_{i_1} \ldots \mathrm{d}\mathbf{r}_{i_{M-1}} \mathrm{d}\mathbf{q}_{i_{M-1}} \times \left\langle \sum_{i_1 > i_2 > \ldots > i_M} \rho_i^{\mathrm{W}}\left(\mathbf{r}_{i_1}, \mathbf{q}_{i_1} \ldots \mathbf{r}_{i_{M-1}}, \mathbf{q}_{i_{M-1}}\right) \right\rangle. \tag{3}$$

In Eq. (3), $\langle ... \rangle$ represents the event averaging; $\mathbf{r}_{i_1}$, ..., $\mathbf{r}_{i_{M-1}}$ and $\mathbf{q}_{i_1}$, ..., $\mathbf{q}_{i_{M-1}}$ are the $M-1$ relative coordinates and momenta in the M-parton rest frame; ρ_i^{W} is the Wigner phase space function inside the hadron, and G is the statistical factor for the M partons.

To determine the quark Wigner phase space functions inside Ω and ϕ, we need quark wave functions. The quark wave functions can be taken as a spherical harmonic oscillator as done in early work [34]. For the ϕ particle, it can be expressed as

$$\psi(\mathbf{r}_1, \mathbf{r}_2) = 1\Big/\left(\pi\sigma_\phi^2\right)^{3/4} exp\left[-\mathbf{r}^2\Big/\left(2\sigma_\phi^2\right)\right], \tag{4}$$

where $\mathbf{r} = \mathbf{r}_1 - \mathbf{r}_2$ is the relative coordinate and σ_ϕ is a size parameter of ϕ. Its normalized wave function leads to a root-mean-square (RMS) radius of $R_\phi = (3/8)^{1/2}\sigma_\phi$. The quark Wigner function in the ϕ particle can be expressed as

$$\rho_\phi^W(\mathbf{r}, \mathbf{k}) = 8exp\left(-\frac{\mathbf{r}^2}{\sigma_\phi^2} - \sigma_\phi^2\mathbf{k}^2\right), \tag{5}$$

where $\mathbf{k} = (\mathbf{k}_1 - \mathbf{k}_2)/2$ is the relative momentum between s and $\bar{s}$.

Similarly, for Ω^- and $\bar{\Omega}^+$ particles, their wave function can be described by the following equation

$$\psi(\mathbf{r}_1, \mathbf{r}_2, \mathbf{r}_3) = \left(3\pi^2\sigma_\Omega^4\right)^{-3/4} \exp\left(-\frac{\rho^2 + \lambda^2}{2\sigma_\Omega^2}\right). \tag{6}$$

The quark Wigner phase space function inside the Ω^- and $\bar{\Omega}^+$ baryon can be expressed as

$$\rho_\Omega^W(\rho, \lambda, \mathbf{k}_\rho, \mathbf{k}_\lambda) = 64 \exp\left(-\frac{\rho^2 + \lambda^2}{\sigma_\Omega^2}\right) \exp\left[-\left(\mathbf{k}_\rho^2 + \mathbf{k}_\lambda^2\right)\sigma_\Omega^2\right], \tag{7}$$

where ρ and λ are relative coordinates of quark, $\mathbf{k}_\rho$ and $\mathbf{k}_\lambda$ are relative momenta, and σ_Ω is a size parameter that is related to the RMS radius, R_Ω.

The two parameters σ_ϕ and σ_Ω in the quark Wigner phase space functions inside the ϕ meson and Ω baryon are related to their RMS radii. We take the same values of RMS, $R_\phi = 0.65$ fm and $R_\Omega = 1.2$ fm, as used in Ref. [34]. One should note that the quark coalescence model violates energy conservation. The effect is much more ambiguous at low p_{T}. In the present study, the coalescence model is considered as a perturbative approach, valid only if the numbers of partons coalesced into hadrons are small compared with the total numbers of partons in the system [34]. This condition is satisfied for Ω and ϕ produced in relativistic heavy-ion collisions because their numbers are indeed significantly smaller than that of kaons.

4 Transverse momentum spectra of Ω and ϕ

Using the parton phase space information and the dynamical quark coalescence model, we first study the effect of local parton density fluctuation on the transverse momentum p_{T} spectra of Ω and ϕ.

Figure 2 presents the transverse momentum distributions of Ω and ϕ at midrapidity ($|y| \leq 1$) in Au + Au

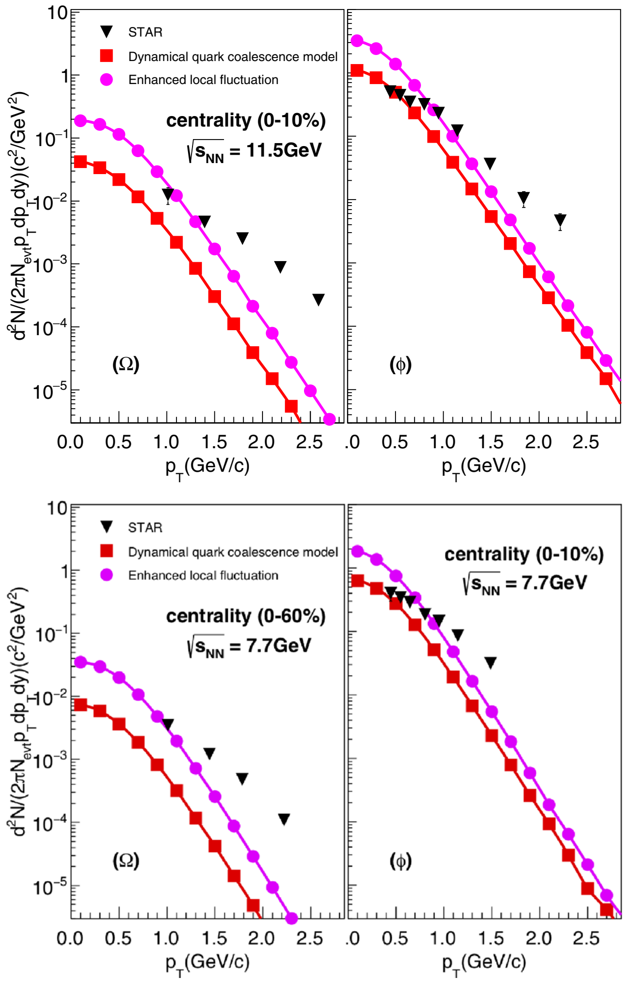

Fig. 2 (Color online) Transverse momentum spectra of Ω and ϕ at midrapidity in Au + Au collisions at $\sqrt{s_{\mathrm{NN}}}$ = 11.5 and 7.7 GeV. The pink circle points are results with enhanced local parton density fluctuation scenarios, while the red square points are results from AMPT with the dynamical quark coalescence model. Black triangle points are experimental data [28]

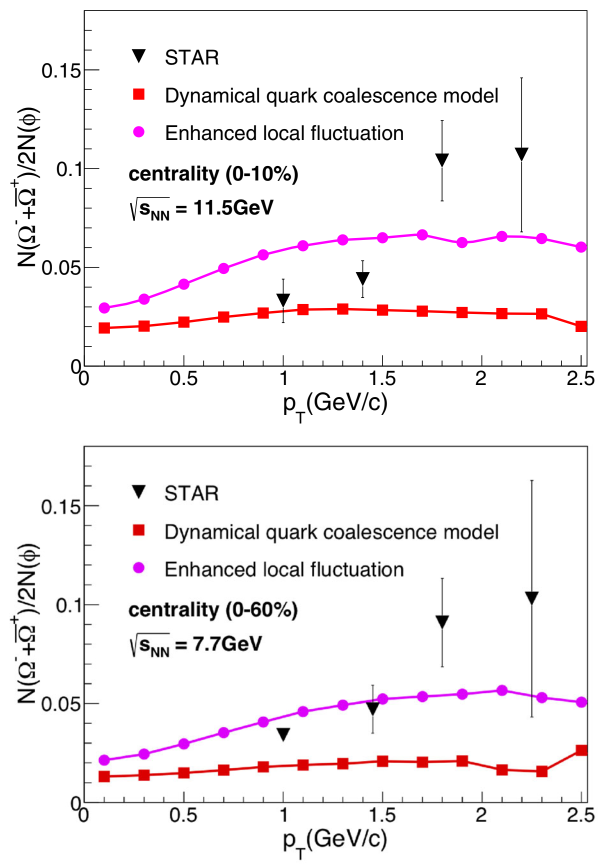

Fig. 3 (Color online) Ratio of Ω to ϕ in Au + Au collisions at $\sqrt{s_{\mathrm{NN}}}$ =11.5 and 7.7 GeV. Pink circle points are calculations from AMPT with enhanced local parton density fluctuation, while red square points are results from AMPT, both with the dynamical quark coalescence model. The original AMPT with the naive quark coalescence model only predicts 20% of the experimental data [30]

collisions at $\sqrt{s_{\mathrm{NN}}}$ = 11.5 and 7.7 GeV. The local parton density fluctuation causes the trend to increase the production rate of Ω and ϕ in comparison with the two AMPT calculations shown in Fig. 2. The fluctuation scenario describes the experimental data better than the original AMPT case, both with dynamical quark coalescence. We note that the calculations at $p_{\mathrm{T}} >$ 1 GeV/c are below the data, particularly for the Ω. Our result is similar to that shown in Ref. [34], which may be attributed to the deficiency of the AMPT model in treating baryon production. Development on this direction is on the way and better description on proton and Λ productions have been achieved [33]. Nevertheless, one should note that the AMPT model with naive quark coalescence only predicts 20% of Ω yield [30]. The new calculation certainly improves the description of Ω and ϕ production.

We further study the ratio of Ω/ϕ as a function of p_{T}, which is believed to be sensitive to local strange quark fluctuation. The results are presented in Fig. 3. The $N(\Omega^- + \bar{\Omega}^+)/2N(\phi)$ ratio from string melting AMPT increases slowly as p_{T} increases. It is close to the experiment data at $p_{\mathrm{T}} <$ 1.0 GeV/c and underestimates the ratio at high p_{T} significantly. For the result from AMPT with enhanced local parton density fluctuation scenario, the ratio is larger and describes the experimental data well, especially for $p_{\mathrm{T}} >$ 1.5 GeV/c. It seems that the density fluctuation scenario allows a larger possibility for strange quarks or antiquarks to overlap in the coordinate space, as shown in Fig. 1. The production rate on Ω and ϕ thus enhances via quark coalescence. The effect is stronger on Ω than ϕ from the Ω/ϕ ratio analysis.

5 Anisotropic flows of Ω and ϕ

In this section, we evaluate the effect of variations in local parton density spatial distributions and discuss its consequence on elliptic flow. The collectivity in high-energy heavy-ion collisions can be measured through final particle azimuthal anisotropy [47]. The anisotropy coefficients are generally obtained from Fourier expansion of final particle azimuthal distortion [48]. i.e.,

$$E\frac{\mathrm{d}^3N}{\mathrm{d}^3p} = \frac{1}{2\pi}\frac{\mathrm{d}^2N}{p_{\mathrm{T}}\mathrm{d}p_{\mathrm{T}}\mathrm{d}y}\left(1+\sum_{i=1}^{N}2v_n\cos[n(\varphi-\psi_{\mathrm{RP}})]\right), \tag{8}$$

where E is the energy of the final particle, p_{T} is the transverse momentum, y is the rapidity, φ is the azimuthal angle of the particle, and ψ_{RP} is the reaction plane angle. The Fourier coefficients, $v_n (n = 1, 2, \ldots)$, can be described by the following equation

$$v_n = \langle\cos(n[\varphi-\psi_{\mathrm{RP}}])\rangle. \tag{9}$$

Similarly, the calculation of harmonic flow, v_n, can be relative to the participant plane angle, $\psi_n\{PP\}$ [47, 48]. For the study of the local parton density fluctuation effect on anisotropy flow, the participant plane method may be more straight forward [49]. The participant plane angle can be defined by the following equation

$$\psi_n\{PP\} = \frac{1}{n}\left[\arctan\frac{\langle r^2\sin(n\varphi)\rangle}{\langle r^2\cos(n\varphi)\rangle}+\pi\right], \tag{10}$$

where n is nth-order participant plane, r and φ are the coordinates position and azimuthal angle of partons, and $\langle\ldots\rangle$ represents parton number density weighting.

Figure 4 shows the v_2 of Ω and ϕ in Au + Au collisions at $\sqrt{s_{\mathrm{NN}}}$= 11.5 and 7.7 GeV. Our results from AMPT with string melting versions and the enhanced local parton density fluctuation scenario are consistent with the experimental data, considering the large statistical uncertainty. Comparing the two sets of AMPT model results, the difference in v_2 is small. It may be because the v_2 is mainly developed in the parton cascade stage in the AMPT model [36]. Another reason may be related to the spatial anisotropy.

The spatial anisotropy is quantified by the participant eccentricity coefficients $\varepsilon_{\mathrm{part}}$ [51, 52]:

$$\varepsilon_2(\mathrm{part}) = \frac{\sqrt{\left(\sigma_y^2-\sigma_x^2\right)^2+4\sigma_{xy}^2}}{\sigma_y^2+\sigma_x^2}, \tag{11}$$

where

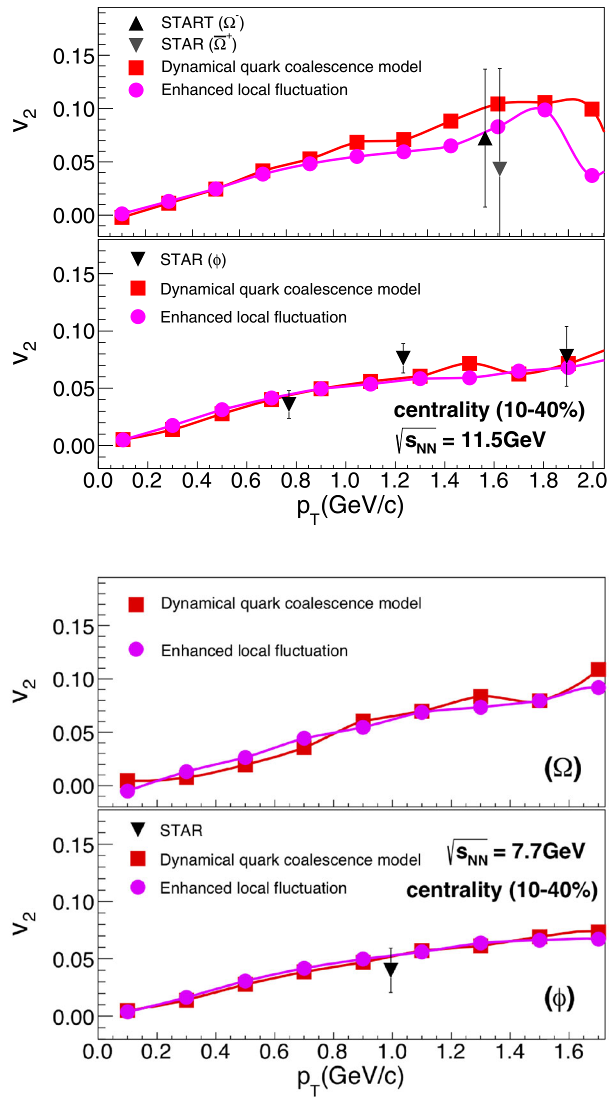

Fig. 4 (Color online) Elliptic flow of Ω (upper panel) and ϕ (bottom panel) as a function of p_{T} in Au + Au collisions at $\sqrt{s_{\mathrm{NN}}}$= 11.5 and 7.7 GeV. Red square points are results from AMPT with dynamical quark coalescence, and pink circle points represent AMPT with enhanced local parton density fluctuation scenario. Experimental data are plotted for comparison [50]

$$\sigma_x^2 = \{x^2\}-\{x\}^2 \tag{12}$$

$$\sigma_y^2 = \{y^2\}-\{y\}^2 \tag{13}$$

$$\sigma_{xy} = \{xy\}-\{x\}\{y\}, \tag{14}$$

and {...} denotes the average over all participants in one event. The results from the AMPT model prior to quark hadronization with different sets of configuration are shown in Fig. 5. It is found that the local parton density fluctuation does not have a large impact on eccentricity.

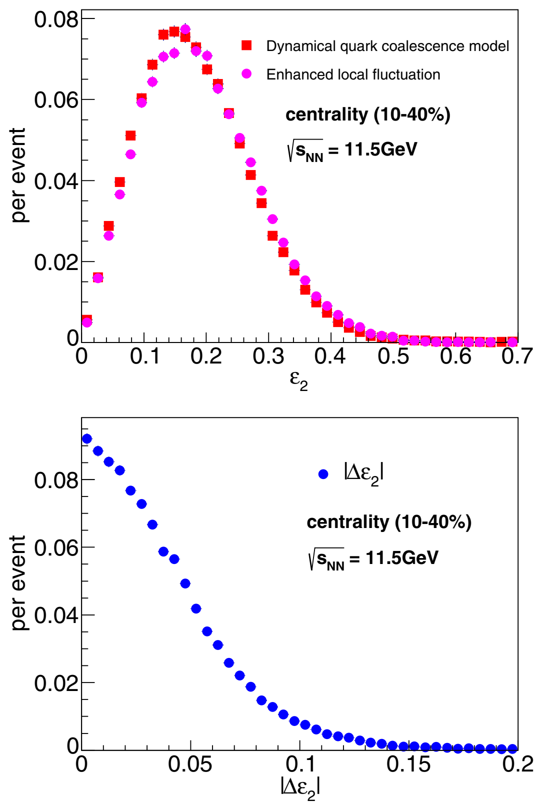

Fig. 5 (Color online) Results of participant eccentricity from the AMPT with and without the enhanced local parton density fluctuation scenario. The upper panel presents the ε_2 distribution and the bottom panel shows the absolute difference $|\Delta\varepsilon_2|$ distribution

6 Summary

In summary, we have studied the local parton density fluctuation effect on Ω and ϕ production in heavy-ion collisions based on the parton phase space information from the AMPT model. We have calculated the transverse momentum spectra, the particle ratio, and the elliptic flow of Ω and ϕ in Au + Au collisions at $\sqrt{s_{\mathrm{NN}}}$= 11.5 and 7.7 GeV. For the production of Ω and ϕ, it is found that the local parton density fluctuation increases the yield more than normal AMPT calculation. Our new results improve the description of experimental data. The increase is more visible in the Ω/ϕ ratio versus p_{T}. For the v_2 of Ω and ϕ, the results are almost the same between the two scenarios of our calculations may be due to small difference of spatial eccentricity between the two scenarios. Our study implies that the Ω/ϕ ratio could provide valuable insight into possible strong density fluctuations pertaining to the search of critical point or first order phase transition in the future Phase II of the BES experiment at RHIC. We note that there are many other observations that may be sensitive to the strong local parton density fluctuation, such as the high moment analysis of conserve quantum number [9]. The study is ongoing and not ready to be published yet.

Acknowledgements We are grateful to Dr. Zi-Wei Lin for the help to implement the local parton density fluctuation effect in AMPT model.

References

1. M.M. Aggarwal et al., arXiv:1007.2613
2. Y. Aoki, G. Endrodi, Z. Fodor et al., The order of the quantum chromodynamics transition predicted by the standard model of particle physics. Nature **443**, 675 (2006). https://doi.org/10.1038/nature05120
3. P. de Forcrand, O. Philipsen, The QCD phase diagram for small densities from imaginary chemical potential. Nucl. Phys. B **642**, 290 (2002). https://doi.org/10.1016/S0550-3213(02)00626-0
4. Z. Fodor, S.D. Katz, Critical point of QCD at finite T and μ, lattice results for physical quark masses. J. High Energy Phys. **4**, 50 (2004). https://doi.org/10.1088/1126-6708/2004/04/050
5. G.Y. Shao, X.Y. Gao, Z.D. Tang et al., QCD phase diagram with the improved Polyakov loop effective potential. Nucl. Sci. Tech. **27**, 151 (2016). https://doi.org/10.1007/s41365-016-0152-0
6. L. Adamczyk et al. (STAR Collaboration), Energy dependence of moments of net-proton multiplicity distributions at RHIC. Phys. Rev. Lett. **112**, 032302 (2014). https://doi.org/10.1103/PhysRevLett.112.032302
7. L. Adamczyk et al. (STAR Collaboration), Beam energy dependence of moments of the net-charge multiplicity distributions in Au + Au collisions at RHIC. Phys. Rev. Lett. **113**, 092301 (2014). https://doi.org/10.1103/PhysRevLett.113.092301
8. L. Adamczyk et al. (STAR Collaboration), Energy dependence of $K\pi$, $p\pi$ and Kp fluctuations in Au + Au collisions from $\sqrt{s_{\mathrm{NN}}}$ = 7.7 to 200 GeV. Phys. Rev. C **92**, 021901(R) (2015). https://doi.org/10.1103/PhysRevC.92.021901
9. X.F. Luo, N. Xu, Search for the QCD critical point with fluctuations of conserved quantities in relativistic heavy-ion collisions at RHIC. Nucl. Sci. Tech. **28**, 112 (2017). https://doi.org/10.1007/s41365-017-0257-0
10. J. Steinhermer, J. Randrup, Spinodal density enhancements in simulations of relativistic nuclear collisions. Phys. Rev. C **87**, 054903 (2013). https://doi.org/10.1103/PhysRevC.87.054903
11. J. Steinhermer, J. Randrup, V. Koch, Non-equilibrium phase transition in relativistic nuclear collisions: Importance of the equation of state. Phys. Rev. C **89**, 034901 (2014). https://doi.org/10.1103/PhysRevC.89.034901
12. F. Li, C.M. Ko, Spinodal instabilities of baryon-rich quark-gluon plasma in the Polyakov–Nambu–Jona-Lasinio model. Phys. Rev. C **93**, 035205 (2016). https://doi.org/10.1103/PhysRevC.93.035205
13. C.M. Ko, F. Li, Density fluctuations in baryon-rich quark matter. Nucl. Sci. Tech. **27**, 140 (2016). https://doi.org/10.1007/s41365-016-0141-3
14. F. Li, C.M. Ko, Spinodal instabilities of baryon-rich quark matter in heavy ion collisions. Phys. Rev. C **95**, 055203 (2017). https://doi.org/10.1103/PhysRevC.95.055203
15. K.J. Sun, L.W. Chen, C.M. Ko et al., Probing QCD critical fluctuations from light nuclei production in relativistic heavy-ion collisions. Phys. Lett. B **774**, 103 (2017). https://doi.org/10.1016/j.physletb.2017.09.056
16. L. Adamczyk et al. (STAR Collaboration), Beam-energy dependence of the directed flow of protons, antiprotons, and pions in Au + Au collisions. Phys. Rev. Lett. **112**, 162301 (2014). https://doi.org/10.1103/PhysRevLett.112.162301
17. S.V. Afanasiev et al. (NA49 Collaboration), Energy dependence of pion and kaon production in central Pb + Pb collisions. Phys.

Rev. C **66**, 054902 (2002). https://doi.org/10.1103/PhysRevC.66.054902
18. C. Alt et al. (NA49 Collaboration), Pion and kaon production in central Pb + Pb collisions at 20*A* and 30*A* GeV: evidence for the onset of deconfinement. Phys. Rev. C **77**, 024903 (2008). https://doi.org/10.1103/PhysRevC.77.024903
19. J. Adams et al. (STAR Collaboration), Scaling properties of hyperon production in Au + Au collisions at $\sqrt{s_{NN}}$ = 200 GeV. Phys. Rev. Lett. **98**, 062301 (2007). https://doi.org/10.1103/PhysRevLett.98.062301
20. B.I. Abelev et al. (STAR Collaboration), Energy and system size dependence of ϕ meson production in Cu + Cu and Au + Au collisions. Phys. Lett. B **673**, 183 (2009). https://doi.org/10.1016/j.physletb.2009.02.037
21. B.I. Abelev et al. (STAR Collaboration), Observation of an antimatter hypernucleus. Science **328**, 58 (2010). https://doi.org/10.1126/science.1183980
22. S. Zhang, J.H. Chen, D. Keane et al., Searching for onset of deconfinement via hypernuclei and baryon-strangeness correlations. Phys. Lett. B **684**, 224 (2010). https://doi.org/10.1016/j.physletb.2010.01.034
23. P. Liu, J.H. Chen, Y.G. Ma et al., Production of light nuclei and hypernuclei at high intensity accelerator facility energy region. Nucl. Sci. Tech. **28**, 55 (2017). https://doi.org/10.1007/s41365-017-0207-x
24. K. Hattori, X.G. Huang, Novel quantum phenomena induced by strong magnetic fields in heavy-ion collisions. Nucl. Sci. Tech. **28**, 26 (2017). https://doi.org/10.1007/s41365-016-0178-3
25. J. Tian, J.H. Chen, Y.G. Ma et al., Breaking of the number-of-constituent-quark scaling for identified-particle elliptic flow as a signal of phase change in low-energy data taken at the BNL Relativistic Heavy Ion Collider (RHIC). Phys. Rev. C **79**, 067901 (2009). https://doi.org/10.1103/PhysRevC.79.067901
26. L. Adamczyk et al. (STAR Collaboration), Observation of an energy-dependent difference in elliptic flow between particles and antiparticles in relativistic heavy ion collisions. Phys. Rev. Lett. **110**, 142301 (2013). https://doi.org/10.1103/PhysRevLett.110.142301
27. L. Adamczyk et al. (STAR Collaboration), Centrality and transverse momentum dependence of elliptic flow of multistrange hadrons and ϕ meson in Au + Au collisions at $\sqrt{s_{NN}}$ = 200 GeV. Phys. Rev. Lett. **116**, 062301 (2016). https://doi.org/10.1103/PhysRevLett.116.062301
28. L. Adamczyk et al. (STAR Collaboration), Probing parton dynamics of QCD matter with Ω and ϕ production. Phys. Rev. C **93**, 021903(R) (2016). https://doi.org/10.1103/PhysRevC.93.021903
29. J.H. Chen, F. Jin, D. Gangadharan et al., Parton distributions at hadronization from bulk dense matter produced in Au + Au collisions at $\sqrt{s_{NN}}$ = 200 GeV. Phys. Rev. C **78**, 034907 (2008). https://doi.org/10.1103/PhysRevC.78.034907
30. Y.J. Ye, J.H. Chen, Y.G. Ma et al., Ω and ϕ in Au + Au collisions at $\sqrt{s_{NN}}$ = 200 and 11.5 GeV from a multiphase transport model. Chin. Phys. C **41**, 084101 (2017). https://doi.org/10.1088/1674-1137/41/8/084101
31. H. van Hecke, H. Sorge, N. Xu, Evidence of early multistrange hadron freeze-out in high energy nuclear collisions. Phys. Rev. Lett. **81**, 5764 (1998). https://doi.org/10.1103/PhysRevLett.81.5764
32. A. Shor, ϕ-Meson production as a probe of the quark-gluon plasma. Phys. Rev. Lett. **54**, 1122 (1985). https://doi.org/10.1103/PhysRevLett.54.1122
33. Y.C. He, Z.W. Lin, Improved quark coalescence for a multiphase transport model. Phys. Rev. C **96**, 014910 (2017). https://doi.org/10.1103/PhysRevC.96.014910
34. L.W. Chen, C.M. Ko, ϕ and Ω production in relativistic heavy-ion collisions in a dynamical quark coalescence model. Phys. Rev. C **73**, 044903 (2006). https://doi.org/10.1103/PhysRevC.73.044903
35. C.M. Ko, *Transport model studies of the baryon-rich quark-gluon plasma formed in heavy ion collisions*. PoS CPOD 2009 (2009), p. 034. https://doi.org/10.22323/1.071.0034
36. Z.W. Lin, C.M. Ko, B.A. Li et al., Multiphase transport model for relativistic heavy ion collisions. Phys. Rev. C **72**, 064901 (2005). https://doi.org/10.1103/PhysRevC.72.064901
37. A. Bzdak, G.L. Ma, Elliptic and triangular flow in *p*-Pb and peripheral Pb–Pb collisions from parton scatterings. Phys. Rev. Lett. **113**, 252301 (2014). https://doi.org/10.1103/PhysRevLett.113.252301
38. Z.W. Lin, Evolution of transverse flow and effective temperatures in the parton phase from a multiphase transport model. Phys. Rev. C **90**, 014904 (2014). https://doi.org/10.1103/PhysRevC.90.014904
39. Z.W. Lin, C.M. Ko, S. Pal, Partonic effects on pion interferometry at the relativistic heavy-ion collider. Phys. Rev. Lett. **89**, 152301 (2002). https://doi.org/10.1103/PhysRevLett.89.152301
40. X.N. Wang, Role of multiple minijets in high-energy hadronic reactions. Phys. Rev. D **43**, 104 (1991). https://doi.org/10.1103/PhysRevD.43.104
41. X.N. Wang, M. Gyulassy, HIJING: a Monte Carlo model for multiple jet production in pp, pA, and AA collisions. Phys. Rev. D **44**, 3501 (1991). https://doi.org/10.1103/PhysRevD.44.3501
42. B. Zhang, ZPC 1.0.1: a parton cascade for ultrarelativistic heavy ion collisions. Comput. Phys. Commun. **109**, 193 (1998). https://doi.org/10.1016/S0010-4655(98)00010-1
43. B.A. Li, C.M. Ko, Formation of superdense hadronic matter in high energy heavy-ion collisions. Phys. Rev. C **52**, 2037 (1995). https://doi.org/10.1103/PhysRevC.52.2037
44. B.A. Li, A.T. Sustich, B. Zhang et al., Studies of superdense hadronic matter in a relativistic transport model. Int. J. Mod. Phys. E **10**, 267 (2001). https://doi.org/10.1142/S0218301301000575
45. Z.W. Lin, C.M. Ko, Partonic effects on the elliptic flow at relativistic heavy ion collisions. Phys. Rev. C **65**, 034904 (2002). https://doi.org/10.1103/PhysRevC.65.034904
46. R. Mattiello, A. Jahns, H. Sorge, H. Stocker, W. Greiner, Deuteron flow in ultrarelativistic heavy ion reactions. Phys. Rev. Lett. **74**, 2180 (1995). https://doi.org/10.1103/PhysRevLett.74.2180
47. J. Ollitrault, Flow systematics from SIS to SPS energies. Nucl. Phys. A **638**, 195 (1998). https://doi.org/10.1016/S0375-9474(98)00413-8
48. U. Heinz, R. Snellings, Collective flow and viscosity in relativistic heavy-ion collisions. Annu. Rev. Nucl. Part. Sci. **63**, 123 (2013). https://doi.org/10.1146/annurev-nucl-102212-170540
49. L. Ma, G.L. Ma, Y.G. Ma, Anisotropic flow and flow fluctuations for Au + Au at $\sqrt{s_{NN}}$ = 200 GeV in a multiphase transport model. Phys. Rev. C **89**, 044907 (2014). https://doi.org/10.1103/PhysRevC.89.044907
50. L. Adamczyk et al. (STAR Collaboration), Centrality dependence of identified particle elliptic flow in relativistic heavy ion collisions at $\sqrt{s_{NN}}$ = 7.7–62.4 GeV. Phys. Rev. C **93**, 014907 (2016). https://doi.org/10.1103/PhysRevC.93.014907
51. B. Alver, G. Roland, Collision-geometry fluctuations and triangular flow in heavy-ion collisions. Phys. Rev. C **81**, 054905, 2010. https://doi.org/10.1103/PhysRevC.81.054905; Erratum: Collision-geometry fluctuations and triangular flow in heavy-ion collisions. Phys. Rev. C **82**, 039903 (2010). https://doi.org/10.1103/PhysRevC.82.039903
52. S. Zhang, Y.G. Ma, J.H. Chen et al., Nuclear cluster structure effect on elliptic and triangular flows in heavy-ion collisions. Phys. Rev. C **95**, 064904 (2017). https://doi.org/10.1103/PhysRevC.95.064904